Journal of Nanobiotechnology

RESEARCH

Open Access

# Macrophage membrane-camouflaged biomimetic nanoparticles for rheumatoid arthritis treatment via modulating macrophage polarization

Renpeng Zhou[1,2,3†], Song Xue[4,5†], Yuanzhi Cheng[2†], Yong Chen[1], Yan Wang[2], Jing Xing[1,2], Hao Liu[1,2], Yucai Xu[1,2], Yi Lin[1,2], Zejun Pei[1,2], Xin Wei[6], Jie Ding[1,2], Shufang Li[1], Ke Wang[1], Feng Yao[1], Yingjie Zhao[1,2,3*], Changhai Ding[5,7*] and Wei Hu[1,2,3*]

## Abstract

Rheumatoid arthritis (RA) is a debilitating autoimmune disease characterized by chronic joint inflammation and cartilage damage. Current therapeutic strategies often result in side effects, necessitating the development of targeted and safer treatment options. This study introduces a novel nanotherapeutic system, 2-APB@DGP-MM, which utilizes macrophage membrane (MM)-encapsulated nanoparticles (NPs) for the targeted delivery of 2-Aminoethyl diphenylborinate (2-APB) to inflamed joints more effectively. The NPs are designed with a matrix metalloproteinase (MMP)-cleavable peptide, allowing for MMP-responsive drug release within RA microenvironment. Comprehensive in vitro and in vivo assays confirmed the successful synthesis and loading of 2-APB into the DSPE-GPLGVRGC-PEG (DGP) NPs, as well as their ability to repolarize macrophages from a pro-inflammatory M1 to an anti-inflammatory M2 phenotype. The NPs demonstrated high biocompatibility, low cytotoxicity, and enhanced cellular uptake. In a collagen-induced arthritis (CIA) mouse model, intra-articular injection of 2-APB@DGP-MM significantly reduced synovial inflammation and cartilage destruction. Histological analysis corroborated these findings, demonstrating marked improvements in joint structure and delayed disease progression. Above all, the 2-APB@DGP-MM nanotherapeutic system offers a promising and safe approach for RA treatment by modulating macrophage polarization and delivering effective agents to inflamed joints.

**Keywords** Rheumatoid arthritis, Membrane-encapsulated nanoparticles, Macrophage polarization, Inflammation, 2-APB

†Renpeng Zhou, Song Xue and Yuanzhi Cheng contributed equally to this work.

*Correspondence:
Yingjie Zhao
zyj@ahmu.edu.cn
Changhai Ding
Changhai.Ding@utas.edu.au
Wei Hu
huwei@ahmu.edu.cn
Full list of author information is available at the end of the article

## Graphical Abstract

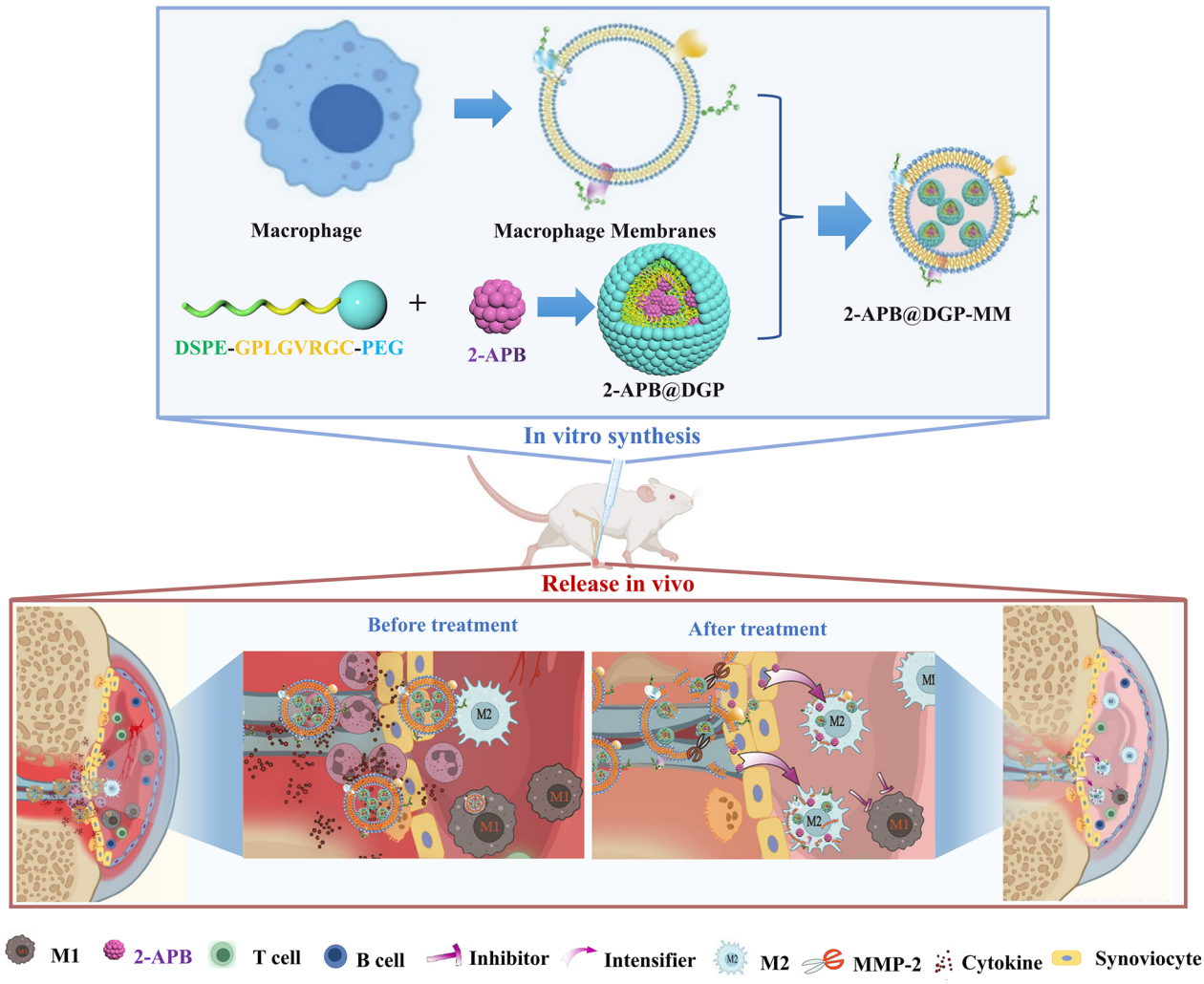


## Introduction

Rheumatoid arthritis (RA) is one of the most prevalent chronic inflammatory diseases, predominantly affecting the whole joints leading to the progressive cartilage destruction and extensive bone erosion [1]. In 2019, 18 million people worldwide had rheumatoid arthritis, and about 70% of those patients were women [2]. Currently, present clinical medications for RA mainly involve four categories of drugs: nonsteroidal anti-inflammatory drugs (NSAIDs), glucocorticoids, nonbiologic disease modifying antirheumatic drugs (DMARDs), and biologic DMARDs [3]. Unfortunately, the majority of these drugs cause numerous serious side effects due to the poor targeting and limitation of administration route, narrowing their clinical application [4]. Therefore, the development of a safer and more effective drug delivery strategy for RA treatment is highly desired.

Innate immune system is widely recognized as the main contributor to the inflammatory response observed in RA, and these associated cells also play a crucial role in activating adaptive immune system. Macrophages are the central to inflammatory processes driving RA synovitis, which constitute the major leucocyte population within the synovial inflammatory infiltrate (≥ 40%) [5]. In RA, the activated macrophages, termed M1 macrophage, produce a series of inflammation cytokines to aggravate joint inflammation [6, 7]. These macrophages are characterized by surface marker expression that includes CD80, CD86 and the release of cytokines and chemokines such as tumor necrosis factor α (TNFα), interleukin-1β (IL-1β) and C-X-C motif chemokine ligand 9 (CXCL9).

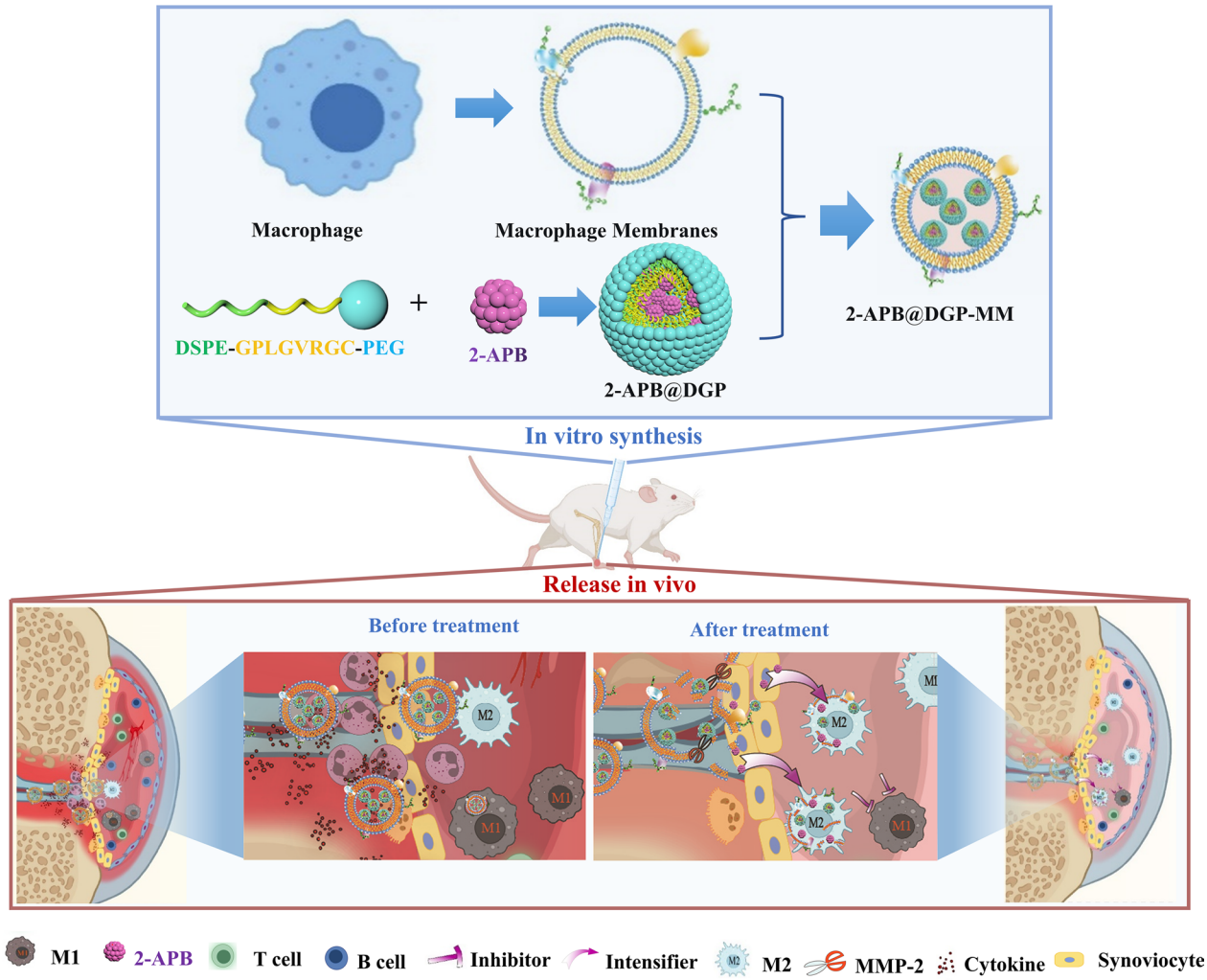


**Scheme 1** Construction of 2-APB@DGP-MM and their inhibition mechanisms of synovial inflammation in rheumatoid arthritis

Conversely, macrophages involved with anti-inflammatory activity and tissue repair are considered to be M2 type, which express surface markers such as CD206, CD209, and CD163 and upregulate the production of cytokines and chemokines such as IL-10 [7–10]. Therapeutically, modulating the macrophage population from a predominance of M1 to M2 in the arthritic RA joints may represent a viable treatment approach.

Boron, as a micro-nutrient, serves for bone synthesis and resorption [11–14], enhancing the absorption of magnesium [15], and diminishing the concentrations of biomarkers involved in systemic inflammation [16, 17]. The most reported biological activity of boron is for boron-containing compounds (BCC). 2-Aminoethoxydiphenylborate (2-APB), as a BCC, has been reported to have a variety of biological functions in multiple systems, such as the immune system, nervous system, and cardiovascular system [11]. Due to its lipophilicity, 2-APB can easily pass through the cell membrane. This property helps 2-APB to reach its different targets [11]. For example, Jonathan G Bilmen et al. reported that 2-APB was an inhibitor of sarco/endoplasmic reticulum $Ca^{2+}$-ATPase (SERCA) $Ca^{2+}$ pumps, and additionally increased ion leakage across the phospholipid bilayer [18]. Notably, 2-APB has been shown to downregulate the levels of pro-inflammatory cytokines like TNF-α and interleukin-6 (IL-6) in immune cell [19–21], and reduce ROS production [22, 23]. Our previous study reported that 2-APB could alleviate the progression of RA by inhibiting the TRPM7 channel to rescue ferroptosis of chondrocytes and could also reduce joint inflammation [24, 25]. These findings lead us to hypothesize whether 2-APB treats RA by modulating macrophage polarization. Interestingly, our preliminary experiments suggest that 2-APB is capable of inhibiting M1 macrophage polarization while promoting M2 macrophage polarization, highlighting its

potential therapeutic value for RA. However, the short half-life and poor water-soluble of 2-APB pose a challenge for its clinical use [26].

The burgeoning field of nanomedicine offers a promising avenue for addressing the limitations of current RA therapies. Nanoparticles encapsulated within natural cell membranes can mimic the properties of parent cells, evade immune clearance and prolong systemic circulation with specific targeting effects [27–30]. Various cell membrane types have been explored for different therapeutic purposes, including those from erythrocytes, stem cells, macrophages, neutrophil and tumor cells [28, 31]. Specifically, macrophage membrane (MM)-encapsulated nanoparticles (NPs) have been shown to exhibit inflammatory site-homing properties due to their characteristic antigenic markers [32]. However, the MM-based NPs for RA therapy need further investigation and have a broad application future.

In this study, our goal in developing the 2-APB@DGP-MM nanotherapy is to harness the targeting capability of MM-encapsulated biomimetic NPs to induce the polarization of macrophages around the RA joint from M1 to M2. This system involves the synthesis of DGPs by ligating DSPE, GPLGVRGC, and PEG molecules; the D-terminus of DGPs is modified to carry 2-APB, while the P-terminus's lipophilic nature facilitates MM encapsulation. The peptide GPLGVRGC, which is specifically cleavable by matrix metalloproteinases (MMPs) in the microenvironment, confers the DGPs with targeted properties (Scheme 1). This innovative nanoplatform, capable of immune system evasion and precise targeting of inflamed joint macrophages, has shown significant promise in ameliorating the progression of RA.

## Methods

### Chemicals and reagents

The chemicals and reagents used in this study were acquired from the following sources: 2-aminoethyl diphenylborinate (2-APB) and Cy5 NHS Ester (Cy5-SE) was obtained from MedChem Express (MCE). 1,2-Distearoyl-sn-glycero-3-phosphoethanolamine-Mal (DSPE-Mal), *N*-hydroxysuccinimide (NHS)-modified poly (ethylene glycol) 2000 Da (mPEG-NHS), and DSPE-mPEG were purchased from Xi'an ruixi Biological Technology Co., Ltd. The matrix metalloproteinases (MMPs)-specific peptide substrate ($NH_2$-GPLGVRGC-SH) was obtained from Sangon Biotech (Shanghai) Co., Ltd. The cell counting kit-8 (CCK-8) was procured from Dojindo Chemical Technology (Shanghai) Co., Ltd. MMP2 was purchased from Pepro-Tech (USA). The Mice macrophage cell line RAW264.7 was obtained from Stem Cell Bank, Chinese Academy of Sciences.

### Cell culture and treatment

RAW264.7 macrophages were plated in 6-well culture plates and were approximately 60–70% confluent. We changed the fresh cell culture medium containing different concentrations of 2-APB (0, 25, 50, 100 μM) and pre-incubated macrophages for 2 h. Finally, the effect of 2-APB on macrophage polarization was observed after co-treatment with LPS (1000 ng/mL) or IL-4 (20 ng/mL) for 24 h.

### Synthesis of the DSPE-GPLGVRGC-PEG (DGP), 2-APB@DGP and 2-APB@DP

$NH_2$-GPLGVRGC-SH was used to connect DSPE-Mal and mPEG-NHS, making it an MMPs-activatable nanosystem. Firstly, DSPE-Mal could react with the sulfhydryl of $NH_2$-GPLGVRGC-SH, producing DSPE-GPLGVRGC. DSPE-GPLGVRGC could further react with the NHS of the mPEG-NHS, producing DSPE-GPLGVRGC-PEG (abbreviated as DGP).

As for the synthesis of 2-APB@DGP, we first added the prepared DGP or DSPE-PEG (abbreviated as DP) (5 mg) into PBS (5 mL). After ultrasound for 10 min, we added 2-APB (100 mM, 10 μL), which dissolved in methylene dichloride in advance, into the above mixture. After stirring and ultrasound, the suspension became clear and further filtered with a 30 KD ultrafiltration tube. The drug content in the supernatant was also detected via ultraviolet (UV). And the drug encapsulation efficiency and loading efficiency were also determined according to the following equation:

$$\text{Encapsulation efficiency} = \text{weight of the loaded drug/weight of the drug in feed} \times 100\%,$$

$$\text{Drug loading efficiency} = \text{weight of the loaded drug/total weight of DGP or DP and the loaded drug} \times 100\%.$$

### Extraction of MM and synthesis of DGP@MM, DP@MM and Cy5-labeled DGP@MM

After cell counting, $5\times10^7$ of RAW264.7 cells were suspended in 1% NP-40 lysis buffer (3 mL) containing phenylmethanesulfonyl fluoride (PMSF). After being incubated in ice for 20 min, the lysis samples were subjected to freeze (liquid nitrogen) and thaw (37 °C) repeatedly three to five times. After that, the suspension was centrifuged at 850×*g* for 15 min, followed by collecting supernatant and centrifuging at 18,000×*g* for 1 h. Finally, the precipitate at the bottom of the tube is the MM. These components can be further cracked via radio immunoprecipitation assay (RIPA) lysis buffer and analyzed its protein quantification via bicinchoninic acid assay (BCA, Beyotime, P0010).

As for DGP@MM synthesis, DGP was mixed with the prepared MM (mass ratio: 1:1), and the mixture was repeatedly squeezed through the 800 nm polycarbonate membrane 15 times to prepare the DGP@MM. Similarly, we prepared DP@MM by coating DP NPs with the prepared MM (mass ratio: 1:1). To prepare the fluorescence-labeled NPs, 2 mg of fluorescent dye Cy5-SE was dissolved in 4 mL of dimethyl sulfoxide (DMSO). Then, the prepared Cy5-SE solution was added to 4 mL DGP solution. After gently stirring for 4 h, the mixture was centrifuged at 12,000 rpm for 3 times (10 min per time) to remove the free Cy5-SE. Then, the prepared MM was used to coat onto Cy5-DGP to obtain the Cy5-DGP@MM.

### Structural characterization, particle size distribution and zeta potential analysis of DGP@MM

The morphology of prepared DGP and DGP@MM were observed using a Transmission Electron Microscope (TEM, JEM-2100), whereas size distribution was obtained via dynamic light scattering (DLS) test and zeta potential performed by a BI-200SM multiangle dynamic/static laser scattering instrument (Brookhaven, USA), respectively. A nuclear magnetic resonance spectrometer (Brooker, AVANCE III HD 400M) and fourier transform infrared spectrometer (FT-IR, IR Affinity 1S) were used to detect the molecular structure and dynamics.

### Matrix-assisted laser desorption/ionization time of flight mass spectrometry (MALDI-TOF/MS)

The analyzer was used at an acceleration voltage + 20 kV. Laser light was focused on the sample using a 8.02 kV lens. A pulsed ion extraction was optimized to 170 ns. MALDI-TOF/MS was ensured on 10 distinct sample deposit zones, and a total of 500 shots were provided.

### High performance liquid chromatograph (HPLC)

HPLC analysis was carried out on an Agilent 1260 system equipped with a YMC-Pack ODS-A column (250 × 4.6 mm, i.d., 5 μm) at 35 °C. The gradient elution mode with acetonitrile–water containing 2% acetic acid as follows: acetonitrile: 0–10 min, 6–6%; 10–20 min, 6–10%; 20–45 min, 10–20%; 45–80 min, 20–35%. The effluent was monitored at 254 nm, and the flow rate was 1.0 mL/min.

### Gel permeation chromatography (GPC)

GPC was utilized for analysis using Agilent PL-GPC50 and PL-GPC220 instruments (New York, USA). After dissolving the samples, organic phase samples were filtered through a 0.45 μm filter membrane, and aqueous phase samples were filtered through a 0.22 μm membrane.

### Cell viability assay

Cytotoxicity of DGP-MM and 2-APB@DGP-MM against RAW264.7 cells and was evaluated via CCK-8 analysis according to the manufacturer's procedures. Specifically, these cells were seeded in 96-well plates at a density of $5\times10^3$ per well. DGP-MM were suspended in culture medium at different concentrations (0, 6.25, 12.5, 25, 50, and 100 μg/mL) and the cells were incubated with these culture mediums for 24 and 72 h, respectively. During the incubation time, the culture medium was refreshed every 24 h. Finally, the cells were incubated with 10% CCK-8 solution for 2 h and subsequently subjected to microplate reader (Spectra Max, Molecular Devices, USA) detection at a wavelength of 450 nm.

Also, we detected the hematotoxicity of DGP-MM or 2-APB@DGP-MM using the fresh red blood cell (RBC) from mice. After incubated with different concentrations of DGP-MM NPs (0, 12.5, 25, 50, and 100 μg/mL), 1% Triton-X 100 (positive control) and sterile PBS (negative control) for 1 h at 37 °C, the RBCs were centrifuged, the OD at 540 nm of supernatant for each sample was further determined with a UV–vis spectrophotometer. The hemolysis percentage = (OD sample − OD negative)/(OD positive − OD negative) × 100%.

### NPs uptake assays in vitro and in vivo

The Cy5-labeled DGP-MM NPs were prepared firstly, then these NPs were incubated with bone marrow-derived macrophages (BMDM) for 4 h. After treatment, the samples were fixed with 4% paraformaldehyde (PFA) and after that stained with DAPI. Finally, these samples were subjected to confocal detection. As for the NPs uptake assay in vivo, the Cy5-labeled DGP-MM and DGP NPs were injected into the ankle joint of the hind legs (5 μL) on DBA/1J mice. After treatment, these mice were

subjected to an in vivo imaging system (IVIS) to determine the residence time in situ.

#### Western blot

Cells were lysed on ice by RIPA buffer (Beyotime, P0013B). Proteins were loaded and separated by 8–10% SDS-PAGE, stained proteins with Coomassie Brilliant Blue (MDTEK, MD5001) or transferred proteins to PVDF membrane (Millipore, IPVH00010) for detection. The PVDF membrane was blocked in 5% non-fat milk and then incubated with corresponding primary antibodies overnight at 4 °C. As for the cell membrane component verification, some important protein markers, such as CD11b (1:2000, Proteintech, P11215, USA), CD49d (1:2000, Proteintech, P13612, USA), F4/80 (1:1000, Cell Signaling Technology, USA) and CD86 (1:1000, Proteintech, P42081, USA), were utilized. Alternatively, the expression of macrophage polarization-related markers iNOS (1:500, Proteintech, 22226-1-AP, USA) and Arg-1 (1:1000, Proteintech, 22226-1-AP, USA) were detected. Then the PVDF membranes were conjugated by peroxidase secondary antibody for 2 h. Finally, the blots were visualized by using an ECL solution, detected with an automatic chemiluminescence imaging analysis system (Tanon, China), and analyzed by Image J software.

#### Quantitative real-time PCR (RT-qPCR)

Cells were harvested and total RNA were extracted with the Trizol reagent (Accurate Biology, AG21102), and transcription-PCR was performed by real-time PCR (AB Stepone). The gene expression was calculated via the $2^{-\Delta\Delta CT}$ method, and *GAPDH* was used as a reference gene. Primers used for RT-qPCR are listed in Table S1.

#### Animal experiment

DBA/1J mice (8–10 week-old) were obtained from the GemPharmatechand feed in the Experimental Animal Center of Anhui Medical University (Hefei, China). All animal experiments were approved by the Animal Ethics Committee of Anhui Medical University (LLSC20190062). The collagen-induced arthritis (CIA) mice model was established as previously described [33]. Specifically, male DBA/1J mice were injected intradermally at the base of the tail with a mixture of 100 μL of emulsion containing 50 μL of chick type II collagen (CII; Chondrex) and an equal volume of Complete Freund's Adjuvant (5 mg/mL; Chondrex). On day 21, a booster injection containing a mixture of 100 μL of an emulsion 100 μg of chick CII, and an equal volume of Incomplete Freund's Adjuvant (Chondrex) was given intradermally at the base of the tail. Mice were then monitored daily for arthritis progression. Special care was taken to ensure that all mice had adequate access to food and water during disease development.

The CIA mice were divided into 5 groups (n = 8) and the normal healthy mice with saline treatment were used as control. The treatment was started on day 28 after the first immunization, 5 μL of saline, 2-APB (100 μM) and NPs (DGP-MM, 2-APB@DGP and 2-APB@DGP-MM) were injected into each ankle joint of the hind legs every 4 days from day 28 to 49. The hind paw thickness and arthritis index score were recorded every other day.

#### Histological analysis

After treatment, the mice were sacrificed, and the ankle joints and main organs were collected and fixed in 4% paraformaldehyde overnight for 48 h. Ankle joints were decalcified with 10% EDTA solution for 30 days. Samples were embedded in paraffin and sliced into 4 μm-thick sections. Hematoxylin and eosin (H&E) and safranin O-fast green (S/F) staining were performed for the paraffin histological study. In addition, the histological study of heart, liver, spleen, lungs, and kidneys provided evidence for the biosafety evaluation of the above NPs.

#### Immunofluorescence staining

Immunofluorescence staining of Aggrecan (1:200, Thermo Fisher, 1380-1-AP, USA) and Collagen II (1:200, Proteintech, 28459-1-AP, USA) in cartilage was performed to reflect its degradation degree in vivo. The joint samples of the CIA mice were stained with antibody against iNOS (the M1 macrophage marker) and CD206 (the M2 macrophage marker) to determine the anti-inflammatory effect of MM-encapulated NPs in vivo.

#### Arthritis index score and paw thickness measurement

Specific arthritis index scoring criteria is ranked on a 0–4 scale as previously reported [34]: (1) 0 point: no local redness or swelling; (2) 1 point: slight swelling of the knuckles; (3) 2 point: moderate swelling of the ankle or wrist joint; (4) 3 point: severe swelling of the entire foot and claws; (5) 4 point: claws appear stiff or deformed [35]. Electronic vernier calipers were used to measure the toe thickness of the inflammatory joints in mice in each group. The vernier caliper happens to be in contact with the mouse toe skin, ensuring the mouse skin is not squeezed and that the position is the same for each assay.

#### Micro-CT

Ankle bone mass was analyzed by Skyscan 1276. The original data were reconstructed using NRcon to obtain the results, and sample drawing was performed using CTvox software (Skyscan Bruker). Three-dimensional structural parameters including bone volume percentage (BV/TV), bone surface density (BS/TV), trabecular

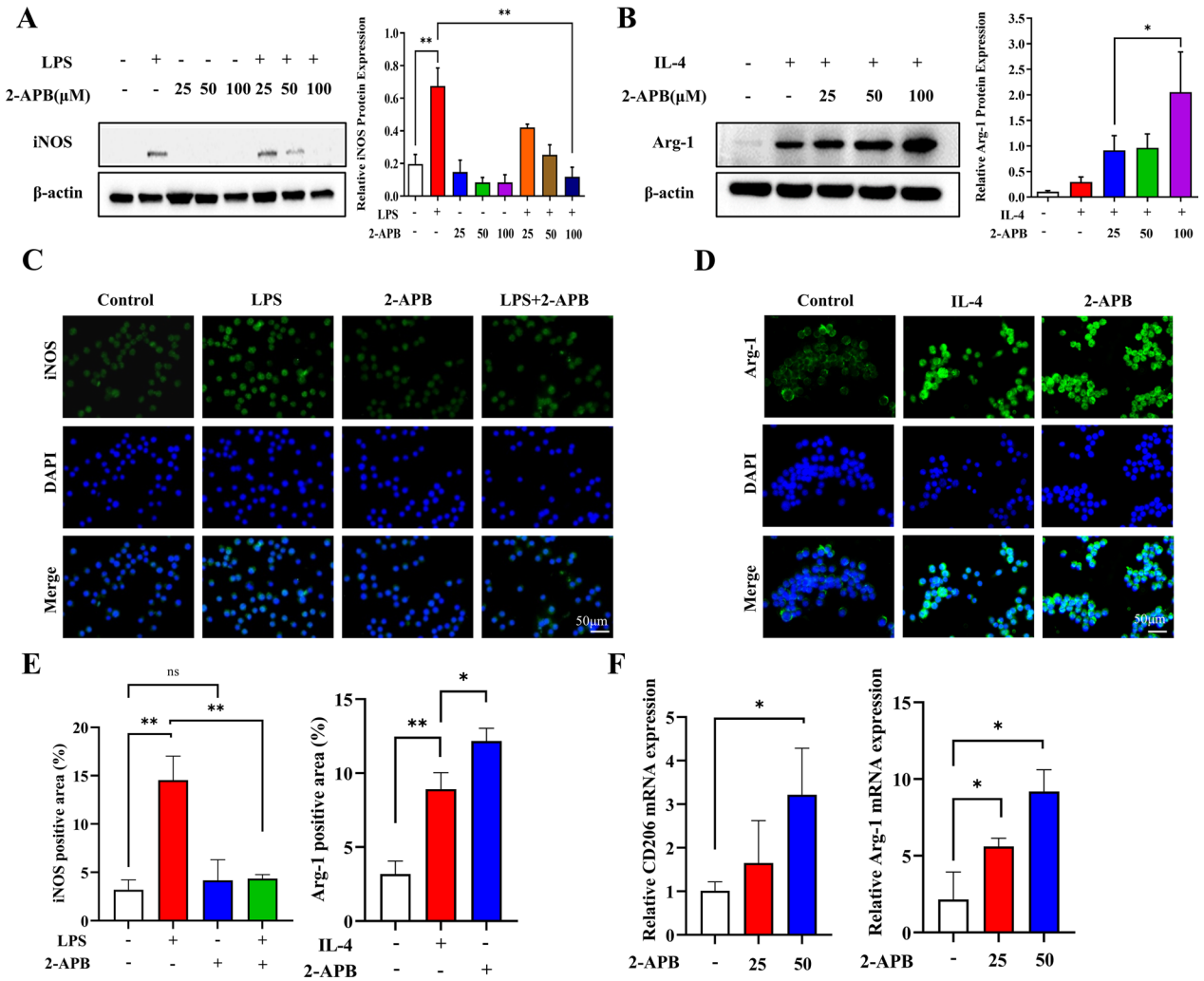


**Fig. 1** 2-APB promotes the phenotypic transformation of macrophages from M1 to M2. **A**, **B** The effect of 2-APB on the expression of polarization marker proteins iNOS and Arg-1 in RAW264.7 cells after LPS/IL-4 treatment. **C**, **D** Effect of 2-APB on the expression of iNOS and Arg-1 on RAW264.7 via confocal fluorescence (scale bar: 50 μm). **E** Quantitative analysis of the iNOS and Arg-1 fluorescence intensity (n = 3). **F** Effect of 2-APB on the expression of *CD206* and *Arg-1* mRNA in RAW264.7. ns = no significance; **P* < 0.05; ***P* < 0.01

thickness (Tb.Th), trabeculae number (Tb.N), and trabecular bone (Tb.Sp) were analyzed.

### Statistical analysis

All results were reported as means ± standard deviation (SD) or mean ± standard error of mean (SEM). Differences between two comparative groups were assessed using the Student's t-test, and the significance among multiple groups was examined by the one-way analysis of variance (ANOVA).

## Results

### 2-APB repolarized M1 type macrophages to M2 phenotype

Macrophages have a high plasticity and can be activated into different subpopulations that are involved not only in the propagation, but also in the inflammation

(See figure on next page.)

**Fig. 2** Synthesis and characterization of DGP-MM and 2-APB@DGP. **A** The synthesis process of DSPE-GPLGVRGC-PEG (DGP). **B** The characteristic peak of DSPE-PEG, GPLGVRGC and DGP in 1H-NMR assay. **C** The characteristic wavelength numbers in the FT-IR assay. **D** TEM images of DGP and DGP-MM (scale bar: 50 nm). **E** Coomassie blue fast staining assay for the MM, DGP and DGP-MM. **F** Western blot detection for the macrophage markers, including CD11b, CD49d, F4/80, and CD86. **G**, **H** The mean particle size and mean zeta potential of MM, DGP, and DGP-MM. **I** The GPC detection of DGP and DGP plus MMP2 (30 ng/mL). ns = no significance; **P* < 0.05; ***P* < 0.01; ****P* < 0.001

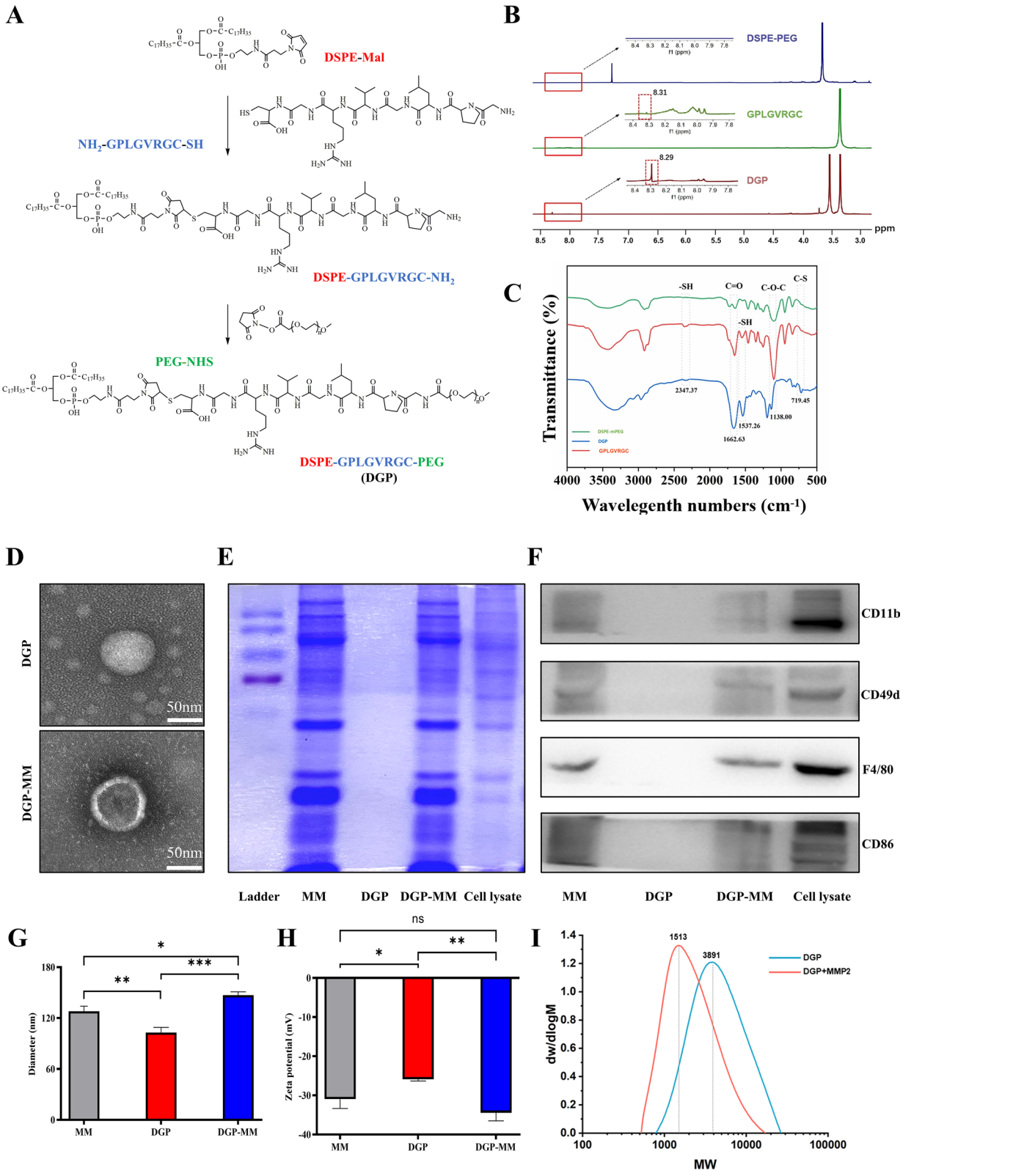


**Fig. 2** (See legend on previous page.)

alleviation, depending on their activation state (M1 or M2) [36]. Therefore, we try to achieve the goal of treating RA by inhibiting the transformation of macrophages into a pro-inflammatory phenotype (M1 type) and promoting their conversion to an anti-inflammatory phenotype (M2 type). To investigate the effect of 2-APB on macrophage polarization, we analyzed the expression of macrophage markers. Based on the western blot results (Fig. 1A, B), 2-APB decreased the expression of M1-related gene *iNOS* and increased the expression of M2-related gene *Arg-1* in a dose-dependent manner. Immunofluorescent observations showed that 2-APB downregulated iNOS positive cell percentage, whereas increased Arg-1 positive cells (M2 macrophage) (Fig. 1C, D). The quantitative analysis results showed that 2-APB significantly inhibited the high expression of iNOS in RAW264.7 cells after LPS stimulation. Meanwhile, 2-APB-treated macrophages upregulated Arg-1 expression than untreated and IL-4-treated cells via fluorescence detection (Fig. 1E). To confirm this result, we measured the mRNA expression of *Arg-1* and *CD206* (Fig. 1F). Collectively, compared to the non-treatment cells, 2-APB could significantly decrease the expression of M1 markers, while increase the M2 markers. These data showed 2-APB could significantly repolarize M1 macrophages to the M2 phenotype. In accordance with our previous report, 2-APB acted as a potentially potent ferroptosis inhibitor to reduce inflammation and rescued RA by inhibiting TRPM7 channels [24]. On the other hand, 2-APB decreased iNOS expression in M1 macrophages and increased Arg-1 expression in M2 macrophages in a concentration-dependent manner, as shown in Fig. 1. iNOS was an enzyme that catalyzed the NADPH-dependent oxidation of L-arginine to produce L-citrulline and nitric oxide (NO). The sustained production of NO triggered inflammation and induced macrophage migration [37]. Nevertheless, the Arg-1 enzyme converted L-arginine to urea and L-ornithine. By degrading arginine, Arg-1 occupied the substrate of iNOS and downregulated NO production. Therefore, inhibition of NO release may also be a mechanism by which 2-APB regulates macrophage polarization.

#### Characterization of 2-APB@DGP-MM

The main synthesis procedure is shown in Fig. 2A, the MMPs cleavable peptide, $NH_2$-GPLGVRGC-SH was used to connect DSPE-Mal and mPEG-NHS, and the prepared DSPE-GPLGVRGC-PEG (DGP) was subjected to MALDI-TOF/MS, nuclear magnetic resonance spectroscopy (NMRS) and FT-IR analysis. Indeed, the MALDI-TOF mass spectrometry was carried out to determine the relative molecular alterations between DGP and DP. As shown in Fig. S1A, the molecular weight of basic substance DSPE-mPEG is about 2814.92 Da. Then GPLGVRGC with a molecular weight of about 884 Da was introduced into DSPE-mPEG, forming a product with 3587.338 Da and being in line with our expectations (Fig. S1B). After the addition of MMP2 (30 ng/mL) to DGP, a product with an approximate molecular weight of 2918.104 Da was observed. This product may be resulted from enzyme shearing. The newly emerging molecular weight was close to mPEG-GPLGVRGC after removal of DSPE fragment (Fig. S1C). Furthermore, the characteristic peak of GPLGVRGC in 1H-NMR assay was shown at 8.31 ppm, while the obvious characteristic peak was also found at 8.29 ppm for DSPE-GPLGVRGC-mPEG (Fig. 2B). In addition, the wavelength numbers in the FT-IR assay were also shown in the Fig. 2C. Combined with MALDI-TOF mass spectrometry results, we can conclude the successful combination of GPLGVRGC and DSPE-mPEG.

To further confirm the macrophage membrane coating effect, we first detected the morphology of DGP and DGP-MM via TEM. As shown in Fig. 2D, DGP and DGP-MM NPs share similar core morphology, however, the latter has a unique core–shell structure. Moreover, the DGP-MM NPs display the same protein profile as MM (Fig. 2E), which is included in the whole cell lysate. DGP-MM NPs also showed similar key macrophage surface biomarkers expression as MM, including CD11b, CD49d, F4/80, and CD86 (Fig. 2F), further demonstrating the successful cell membrane coating effect.

As shown in Fig. 2G, the DGP-MM NPs bear a mean particle size of about 147 ± 4.526 nm, relatively larger than the DGP NPs (128 ± 6.346 nm) and MM (103 ± 6.036 nm). Similarly, the prepared DGP-MM NPs, DGP NPs, and MM equally displayed the negative surface zeta potential, among which the DGP-MM NPs had the highest negative potential (Fig. 2H).

Above all, it is demonstrated that DGP-MM NPs was successfully synthesized. Based on these, we further loaded the 2-APB to delivery into macrophages in vitro and the inflammatory joint in vivo. As demonstrated in Fig. S3, the UV absorption spectrum results showed that 2-APB@DGP (213 ± 5 nm and 275 ± 3 nm) had both characteristic features of 2-APB (213 ± 5 nm) and DGP (275 ± 3 nm), revealing the successful loading of 2-APB in DGP NPs.

#### 2-APB@DGP-MM NPs improves macrophage uptake efficiency, prolong drugretention time with high biological safety

After synthesis and characterization of 2-APB@DGP-MM NPs, we detected their biosafety via CCK-8 assay. As shown in Fig. 3A, after being treated with different concentrations of DGP-MM NPs and 2-APB@DGP-MM

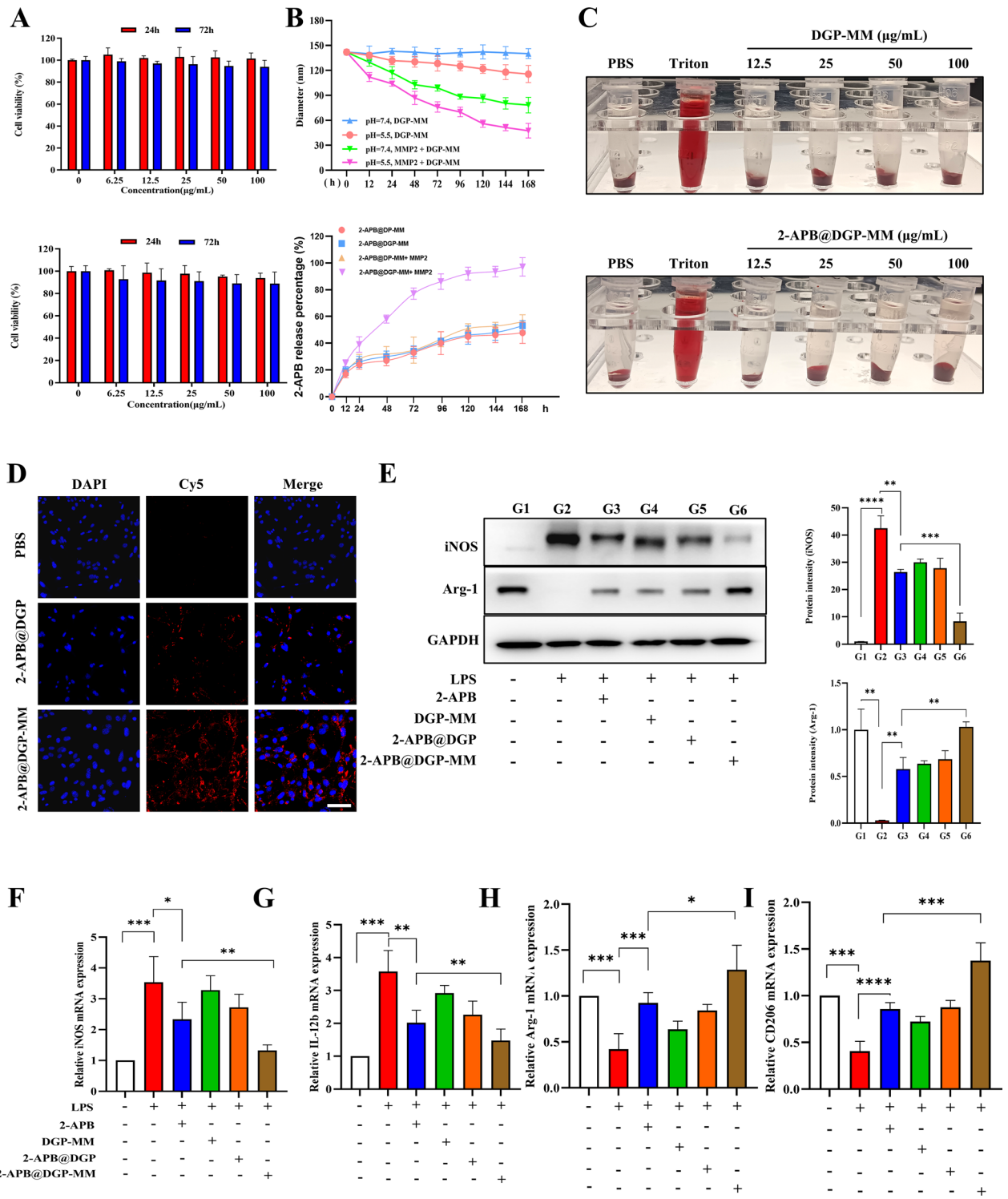


**Fig. 3** 2-APB@DGP-MM promotes macrophage polarization from M1 to M2 via enhancing cellular uptake and drug release. **A** The effects of DGP-MM and 2-APB@DGP-MM on cell viability at different time points and concentrations. **B** The mean diameter alteration of different NPs at different pH conditions after incubation for various time, and the release percentage of 2-APB from different groups at different times. **C** Hematotoxicity of DGP-MM or 2-APB@DGP-MM on the fresh red blood cell from mice at different concentrations of DGP-MM NPs or 2-APB@DGP-MM NPs (0, 12.5, 25, 50 and 100 μg/mL), 1% Triton-X 100 (positive control) and sterile PBS (negative control) for 1 h. **D** The uptake efficiency of Cy5-loaded 2-APB@DGP or Cy5-loaded 2-APB@DGP-MM in BMDMs (scale bar: 40 μm). **E** The protein expression of iNOS and Arg-1 after different treatments for 4 days. **F**–**I** The relative mRNA expression of M1 polarization markers (*iNOS* and *IL-2b*) and M2 polarization markers (*Arg-1* and *CD206*) after corresponding treatments. *$p < 0.05$; **$P < 0.01$; ***$P < 0.001$; ****$P < 0.0001$

NPs for 24 h or 72 h, no significant change after being treated with DGP-MM NPs and 2-APB@DGP-MM NPs at the same concentration and the same time point. Similarly, there was no significant hematotoxicity after incubating with gradient concentrations of DGP-MM NPs or 2-APB@DGP-MM NPs compared with the 1% Triton-X 100 treatment group (Fig. 3C, Fig. S2). On the other hand, the GPLGVRGC, which was further included in DSPE-PEG (DP) and forming DSPE-GPLGVRGC-PEG (DGP), can be cleaved by MMP2. To determine the cleavability of DGP, the GPC detection was applied, which was better than HPLC analysis, and the molecular change was shown in Fig. 2I. The molecular weight (MW) of dw/dlogM peak for DGP and DGP plus MMP2 was about 1513 and 3891, respectively. This result showed the significant decrease of MW after co-incubation with MMP2, demonstrating the MMP2-responsive effect of DGP.

We further incubated 2-APB@DGP-MM NPs in different pH and MMP2-containing mediums (30 ng/mL) for evaluating their bio-stability as demonstrated in Fig. 3B. We can conclude that weak acidic microenvironment accelerates the degradation of macrophage membrane coated NPs. This rapid release was mainly attributed to the fact that macrophages themselves were more sensitive to environmental acidity than alkalinity [38]. Wu et al. reported that macrophage morphology changed to an elongated spindle-shaped shape that was more prone to rupture when the environmental pH decreased from 7.4 to 6.2 [39]. Additionally, as previously reported, several critical cellular functions such as membrane-associated enzyme activities, ion transport activity, and protein and DNA syntheses got weaken at acidic environment, which affected cell morphology and accelerating the degradation of cell membranes [40, 41]. After incubating with MMP2, the degradation rate of DGP-MM NPs was promoted significantly.

The uptake efficiency detection was also performed to investigate the internalization ability of NPs in macrophages. We incubated BMDMs with Cy5-loaded 2-APB@DGP and 2-APB@DGP-MM NPs (or Cy5-DGP and Cy5-DGP-MM NPs) for 4 h. As a result, the intracellular uptake of 2-APB@DGP and 2-APB@DGP-MM NPs (or DGP and DGP-MM NPs) varied according to the different fluorescent intensity of BMDMs (Fig. 3D, S4). That is to say 2-APB@DGP-MM dramatically promoted cellular internalization in macrophages compared with 2-APB@DGP NPs treatment group. We could conclude that macrophage membrane coating (DGP-MM group) dramatically promoted cellular internalization in macrophages compared with DGP NPs treatment group. Furthermore, we have performed in vivo fluorescence imaging for sequential four days. Specifically, Cy5-loaded 2-APB@DGP-MM and 2-APB@DGP NPs were injected into the ankle joint (5 μL) and subjected to IVIS imaging to determine the residence time in situ. As shown in Fig. S5, we found that the membrane coating dramatically extended the whole NPs residence time compared with the no coating group.

The 2-APB release manner from 2-APB@DGP-MM NPs was also determined by HPLC. After indicated incubation time, the supernatant was collected and subjected to HPLC detection. As shown in Fig. 3B, in the presence of MMP2, the cumulative release of 2-APB from the 2-APB@DGP-MM NPs was gradually increased over 90%, and became stable after 120 h of incubation. However, the 2-APB release from other three groups, including 2-APB@DP-MM, 2-APB@DGP-MM and 2-APB@DP-MM plus MMP2, was relatively lower at any time point compared with 2-APB@DGP-MM plus MMP2 treatment group. In the presence of MMP2, the release of 2-APB from 2-APB@DGP-MM was accelerated owing to the GPLGVRGC peptide segment being able to be clipped. Overall, these MMP2-cleavable NPs wrapped in cell membranes could realize the on-demand release of agents upon reaction with high expression of MMPs in the RA microenvironment. In addition, we calculated the drug loading efficiency and encapsulation rate for 2-APB@DGP and 2-APB@DGP-MM, respectively. The drug loading efficiency of 2-APB@DGP and 2-APB@DGP-MM was 4.53% and 3.79%, respectively, and the agent encapsulation rate was 78.21% and 87.75%, respectively (Table S2).

#### 2-APB@DGP-MM NPs manipulate macrophage polarization

After being pre-treated with different NPs for 6 h, Raw264.7 cells were treated with LPS (1 μg/mL) for four days. After treatment, macrophages were subjected to mRNA and protein extraction, respectively. As previously reported [42], there was a significant change of the M1 and M2 marker gene expression. Similarly, we also found LPS stimulation significantly promoted M1 polarization and inhibited M2 polarization (Fig. 3E). Interestingly, after co-treated with 2-APB, DGP-MM and 2-APB@DGP, the M1 macrophage biomarker expression (*iNOS* and *IL-2b*) was downregulated and the M2 biomarker expression (*CD206* and *Arg-1*) was upregulated compared with LPS stimulation group at varying degrees as shown in Fig. 3F–I. Notably, 2-APB and 2-APB@DGP had essentially the same ability to polarize macrophages. This might be attributed to the fact that 2-APB acting alone and 2-APB@DGP, which had not been enveloped by the macrophage membrane, could only enter and interact with macrophages based on their own lipophilic physical properties. On the other hand, given that macrophages were inflammation- and

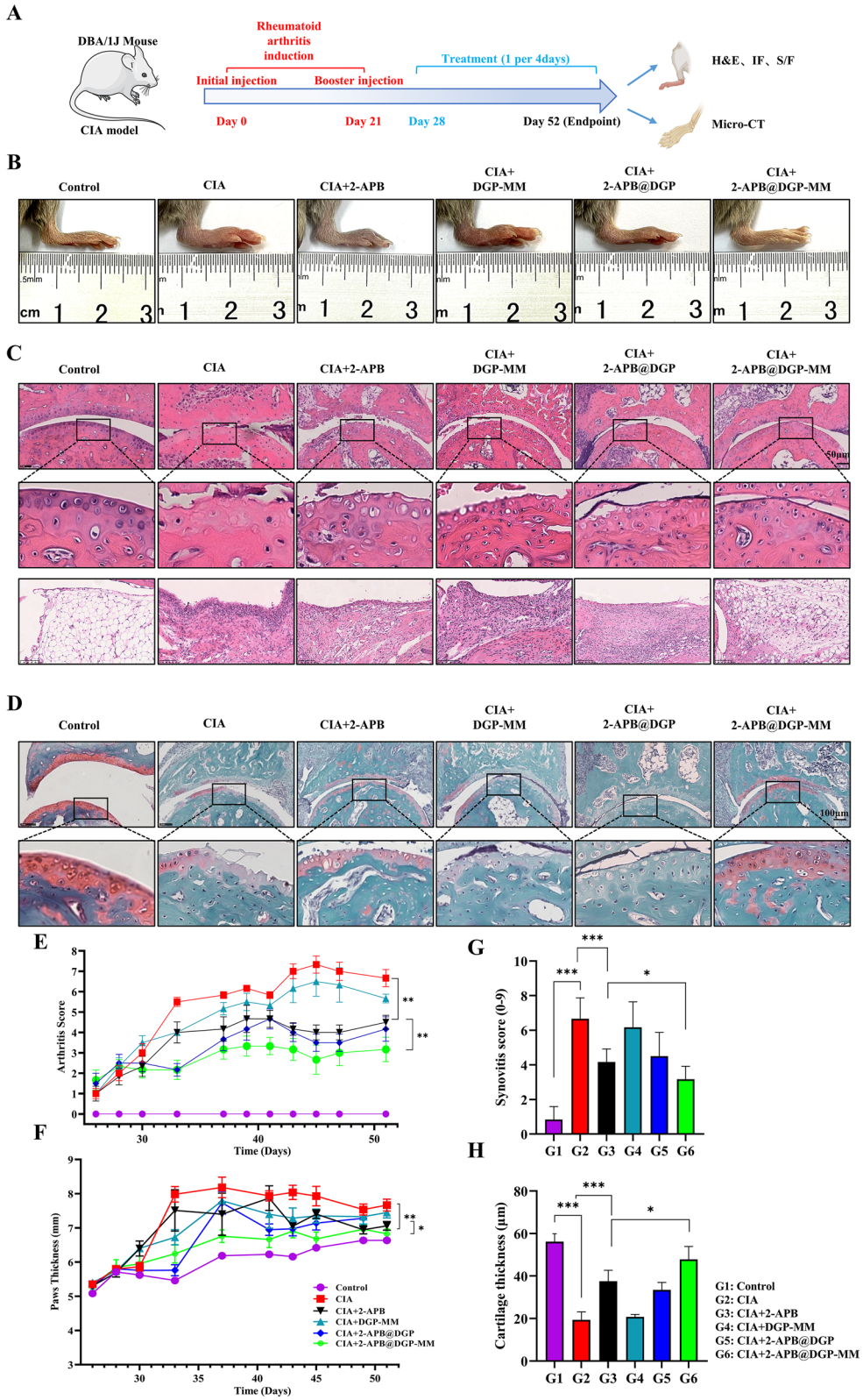


**Fig. 4** 2-APB@DGP-MM inhibits CIA progression. **A** Schematic diagram of treatment schedule. **B** Representative photographs of mice ankle joints after 2-APB@DGP-MM treatment. **C** H&E and **D** S/F staining of ankle joints or synovium from mice after different treatments. **E** The arthritis scores were calculated for the inflammatory joints with different treatments. **F** The paw thickness of the inflamed joints for different treatments. **G** Statistical analysis for the synovitis score and cartilage thickness after different treatments. $^{*}P < 0.05$; $^{**}P < 0.01$; $^{***}P < 0.001$

immune-associated cells that showed chemotaxis and selective binding [43, 44], 2-APB@DGP-MM with macrophage membrane coating was allowed to bind tightly to target cells. Therefore, 2-APB@DGP-MM could be considered to have a greater potential for modulating macrophage polarization. Interestingly, DGP-MM slightly rescued LPS-induced M1 polarization mainly owing to the macrophage membrane neutralizing cytokines and eliminating inflammation. As a typical effector cells, macrophage cells membrane can not only adsorb endotoxin, but also receive inflammation cytokines [45]. Neutralization of inflammatory cytokines could effectively

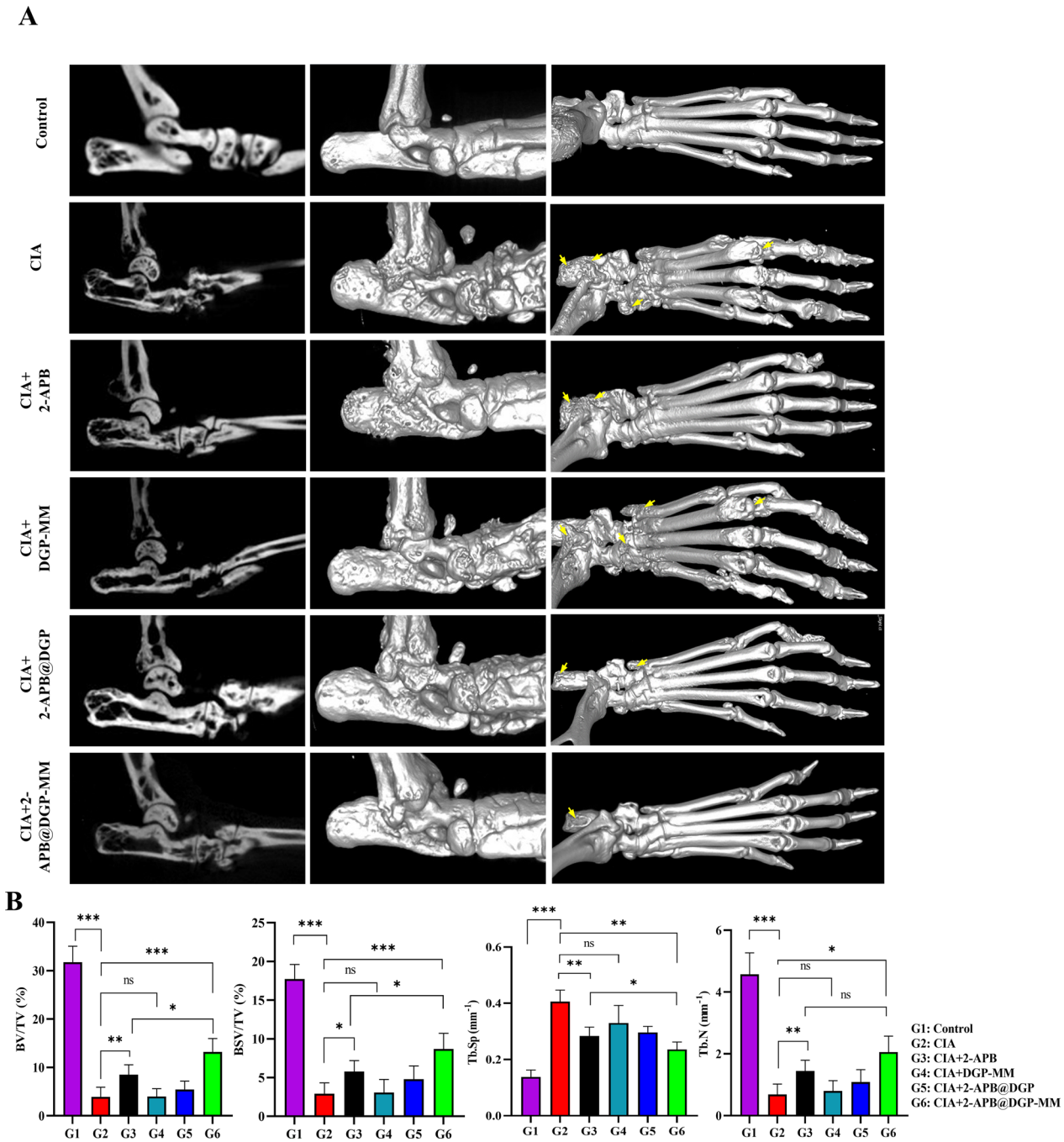


**Fig. 5** 2-APB@DGP-MM alleviates joints destruction in CIA mice. **A** Micro-CT images of ankle joints of CIA mice after 2-APB@DGP-MM, 2-APB@DGP, DGP-MM or 2-APB treatment. **B** Quantitative analysis of the BV/TV, BS/TV, Tb.Sp and Tb.N. ns = no significance; *$P < 0.05$; **$P < 0.01$; ***$P < 0.001$

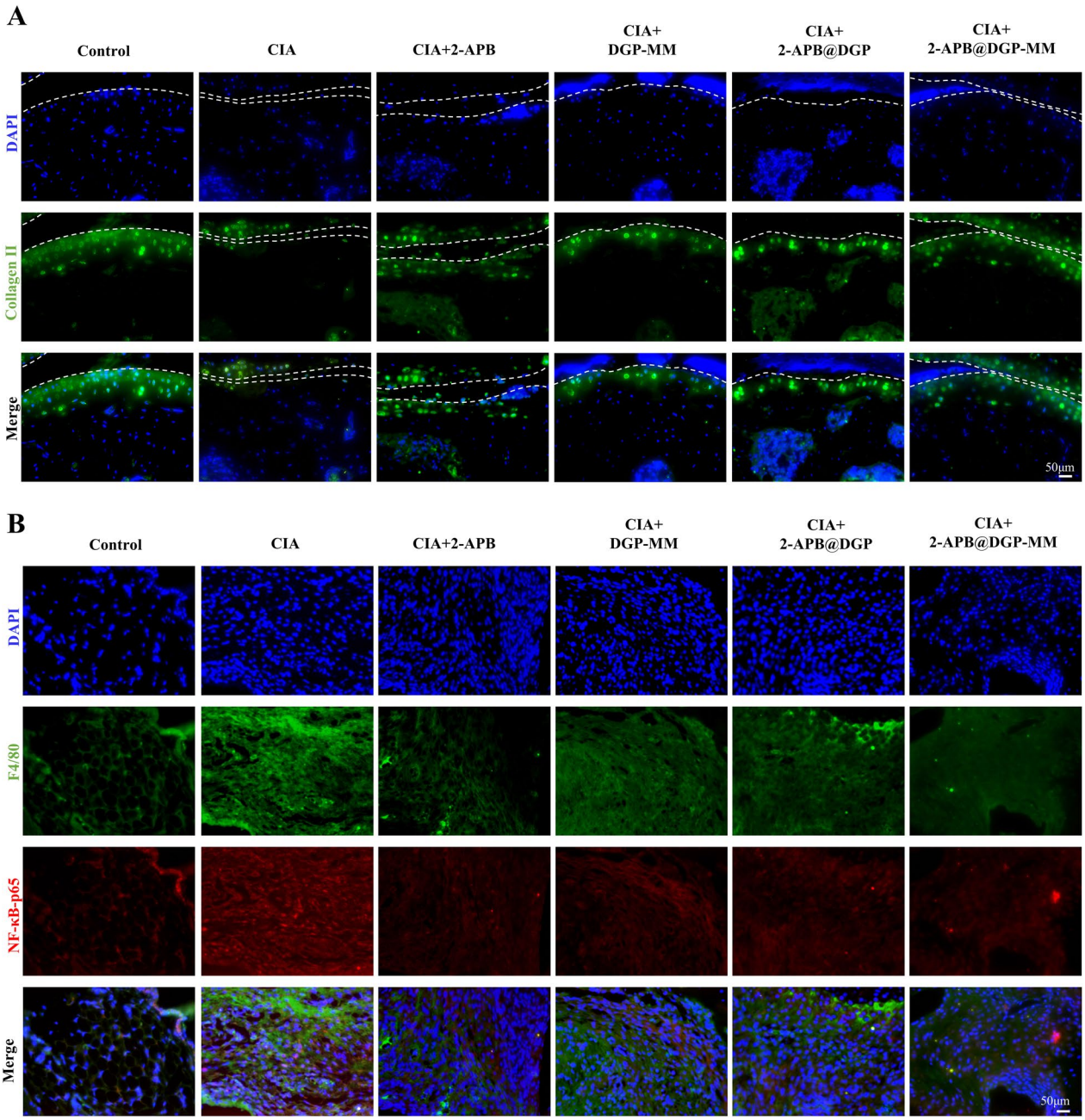


**Fig. 6** 2-APB@DGP-MM restores the level of collagen II and reduces the level of NF-κB-p65 in the joints of CIA mice. Representative fluorescence images of Collagen II (**A**) and NF-κB-p65 (**B**) in the joint tissues after different treatments (scale bar: 50 μm)

prevent innate and adaptive immune cells recruitment and inhibit inflammation induced cartilage destruction, which in turn prevent joint damage [46–48]. Based on the above analysis, 2-APB@DGP-MM can not only effectively absorb and neutralize a large number of inflammatory factors from the environment with the help of macrophage coating on the surface, but also achieve targeted drug delivery with macrophage membrane coating, thereby more effectively promoting M2-type macrophage polarization and achieving a more ideal therapeutic effect. In particular, the 2-APB@DGP-MM co-treatment dramatically rescued the LPS-stimulation effect and significantly reduced inflammation-related gene expression, demonstrating their therapeutic potential for RA.

### 2-APB@DGP-MM NPs modulate macrophage polarization and alleviate cartilage destruction in CIA mice

The efficacy of the above NPs in vivo was investigated in the collagen-induced arthritis (CIA) model of DBA/1J mice. To test whether MM modification can prolong the residence time of NPs and thus achieve better therapeutic outcomes, we injected different drugs every 4 days. The timetable for induction and treatment of arthritis

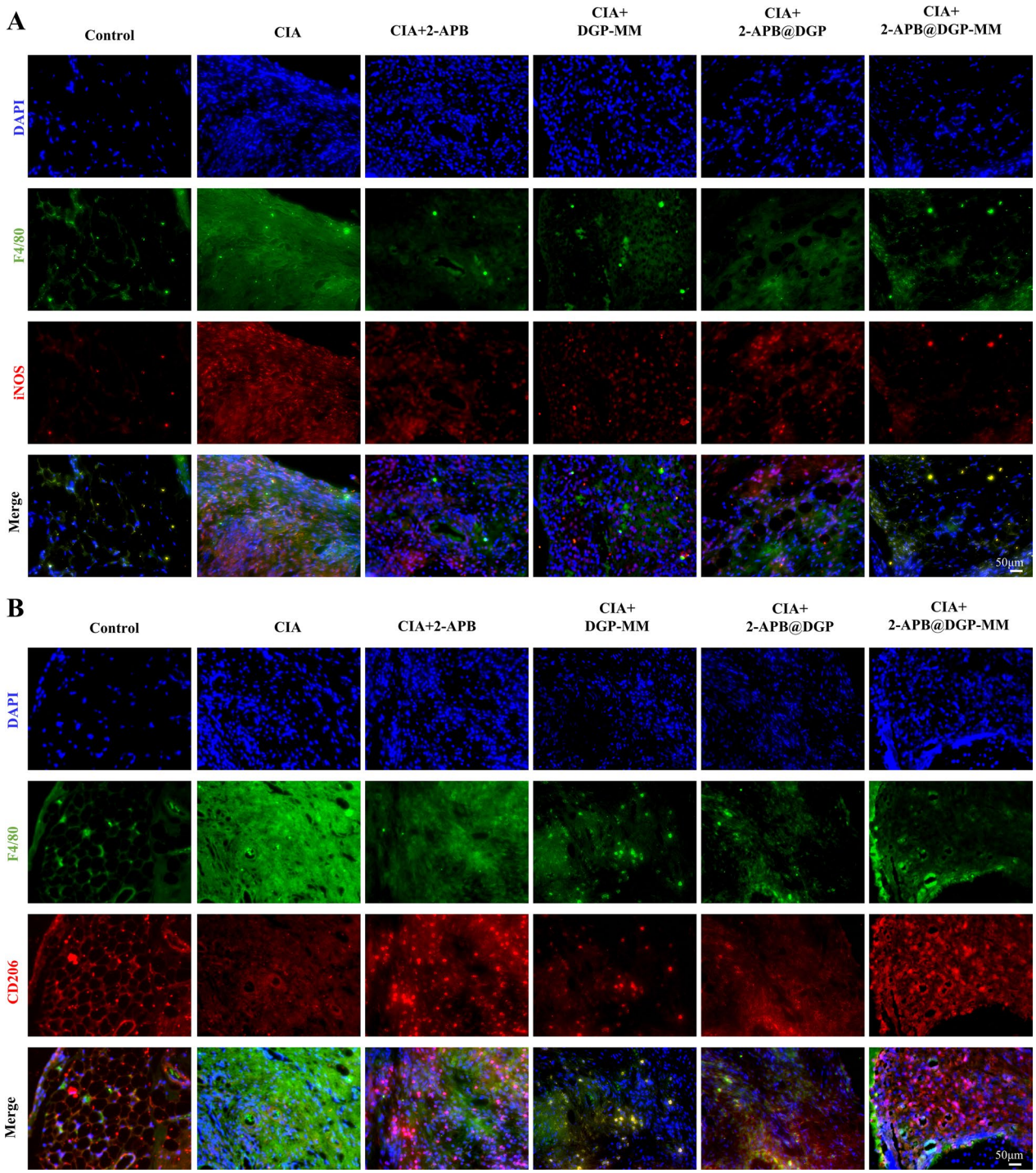


**Fig. 7** 2-APB@DGP-MM modulates macrophage polarization in CIA mice joint. Representative fluorescence images of the co-localization of iNOS (**A**) and CD206 (**B**) with macrophage, respectively, in the joint after different treatment (scale bar: 50 μm)

is shown in Fig. 4A. At the end of treatment, compared with the saline-treated mice, the mice subjected to each formulation showed obvious improvement in the degree of swelling as well as much less redness except for the DGP-MM group (Fig. 4B). Joint swelling was assessed every other day starting at day 21. Arthritis scores for paws gradually increased in saline-treatment animals as the disease progressed, while this progression was slower in animals treated with naked 2-APB, 2-APB@DGP and 2-APB@DGP-MM. It is worth mentioning that the effect of the last group is more pronounced (Fig. 4E). Besides, we performed fluorescence detection of cartilage slides. Specifically, after the articular injection of Cy5-loaded 2-APB@DGP and 2-APB@DGP-MM NPs for 24 h, the joint was collected and subjected to fluorescence detection. We applied F4/80 antibody to label synovial macrophage and FITC fluorescent secondary antibody for visualization. As shown in Fig. S6, the fluorescence signal in Cy5-loaded 2-APB@DGP-MM treatment group is scarcely detected in cartilage. However, the Cy5-loaded 2-APB@DGP-MM can be uptaken more by synovial macrophage (FITC labeled) compared to Cy5-loaded 2-APB@DGP treatment group, indicating the MM-coated NPs could penetrate into synovium and were further uptaken by macrophages, rather than stay in the articular cavity or penetrate into cartilage.

To further validate the therapeutic effect of macrophage membrane-camouflaged NPs on CIA mice, we performed histological analysis of ankle sections from mice in each group using H&E and S/F staining. The degree of cartilage injury and destruction in the CIA group was significantly higher than that in the control group, while the 2-APB, 2-APB@DGP and 2-APB@DGP-MM groups alleviated the damage to varying degrees, and it is worth mentioning that the effect of the 2-APB@DGP-MM group was the most significant (Fig. 4C, D). Consistent with these results, this phenomenon is also observed in the thickness of the ankle cartilage in mice (Fig. 4H). This is almost consistent with the results we observed for the degree of swelling of the ankle joints in the mice in each group (Fig. 4F). The above results suggest that 2-APB and 2-APB@DGP-MM can effectively inhibit the progression of RA.

Bone destruction has emerged as the key milestone during RA progression, indicating its severity and prognosis [49]. Therefore, we investigated joint destruction by Micro-CT which displayed that ankle joints in the sham group still held a rough bone surface and severe bone erosion (yellow triangles) after treatment. We found that treatment with 2-APB@DGP-MM effectively alleviated the cartilage and bone destruction in CIA mice (Fig. 5A). Quantitative results showed that RA decreased the BV/TV, BS/TV, Tb.N and Tb.Th compared with those of healthy mice, indicating significant bone destruction caused by RA, 2-APB@DGP-MM had shown better results in salvaging these injuries (Fig. 5B).

Cartilage destruction and synovitis are also primary pathological features of RA [26]. However, chondrocytes lack specific surface markers; therefore, aggrecan and collagen II are currently the primary indicators used to determine whether there is a chondrocyte biological phenotype. As demonstrated in Fig. 6A, S7, the expression of collagen II (green fluorescence) and aggrecan (red fluorescence) significantly decreased in both the CIA group and the DGP-MM group compared to the control group. Conversely, in the 2-APB@DGP-MM group, there was a substantial increase in the expression of collagen II and aggrecan, indicating a potential cartilage-protective effect. The specialized structure of the lining layer was filled with macrophages and FLS, while the sub-lining layer mainly consisted of vascularized connective tissue [50].

Synovial macrophages and infiltrating monocyte-derived macrophages are essential cells for the development and chronicity of synovitis in RA [36]. Therefore, we further assessed the progression of synovitis by measuring the expression of macrophages in ankle sections of mice in each group. As a result, the positive expression level of NF-κB p65 and iNOS in the CIA group were the highest among the six groups. However, among 2-APB, 2-APB@DGP and 2-APB@DGP-MM treatment groups, the above indicator expression pattern was reversed at different levels (Fig. 6B, 7A). Meanwhile, CD206, a marker for M2 type macrophages, had the highest fluorescence intensity in 2-APB@DGP-MM group (Fig. 7B). The expression of these related markers in articular synovial macrophages suggests that 2-APB@DGP-MM can alleviate the inflammatory response in RA joints. Furthermore, we observed the H&E staining of the synovial membrane of the joints and found that 2-APB@DGP-MM was effective in inhibiting synovitis (Fig. 4C, G). These evidence suggest that the 2-APB@DGP-MM nanotherapeutic system has rescued articular cartilage damage and synovitis in CIA model mice, and further illustrates its potential for the treatment of RA.

Furthermore, no significant systemic toxicity and important organs (heart, liver, spleen, lungs, and kidney) injury in mice after various sample administrations was observed according to the results of H&E staining (Fig. S8). This result verified that DGP-MM, 2-APB@DGP and 2-APB@DGP-MM had no obvious toxicity to the main organs, demonstrating their good biocompatibility. This undoubtedly provides valuable insights for further research and application of 2-APB@DGP-MM NPs.

## Discussion

RA is an autoimmune disorder affecting approximately 1% of the global population, characterized by chronic inflammation leading to joint pain, extensive joint damage, and eventual disability of synovial joints [51]. One of the hallmarks of RA is the uncontrolled proliferation and migration of various cell types, such as fibroblasts, T cells, B cells, neutrophils, and monocytes, into the synovium. These immune-associated cell types are driving forces behind synovial inflammation and pannus formation [52, 53].

Macrophages, as the most abundant immune cells in the synovium, play a critical role in RA progression. Upon activation, macrophages secrete pro-inflammatory cytokines, such as TNF-α and IL-1, which promote the recruitment of immune cells to the inflamed site and enhance the expression of adhesion molecules on endothelial cells [54]. Macrophages also release chemokines, such as MCP1 and IL-8, which attract more immune cells into the RA joint. TNF-α and IL-1 stimulate synovial fibroblasts to express additional cytokines, chemokines, and growth factors. TNF-α also participates in activating and differentiating osteoclasts, which are cells responsible for bone resorption, while IL-1 accelerates chondrocytes to produce MMPs that degrade cartilage [55]. Given the central role of macrophages in both initiation and progression of RA, targeting macrophage polarization is a potential therapeutic strategy for RA management.

2-APB, a boron-containing compound, was found to reduce the levels of inflammatory cytokines in rat bone marrow-derived mast cells, including IL-6, C-reactive protein and fibrinogen [23]. The reduction in IL-6 levels is a key step in modulating inflammatory lesions, including RA and edema in remitting seronegative symmetrical synovitis with pitting edema syndrome [21]. Our research has uncovered that the 2-APB could mitigate joint damage and local inflammation in RA. This may be due to the role of 2-APB as a potential potent ferroptosis inhibitor [24]. In this study, we found that 2-APB significantly inhibited the polarization of pro-inflammatory M1 macrophages and promoted their polarization towards the anti-inflammatory M2 phenotype. This finding expands our understanding of the therapeutic potential of 2-APB.

RA is usually accompanied by synovial hyperplasia and pannus formation, both of which increase the permeability of the synovial sublining layer's capillaries and subsequent infiltration of mononuclear cells, especially macrophages. This heightened permeability accelerates the elimination of therapeutic drugs, thereby shortening their duration in situ [56]. Such enhanced drug clearance poses a formidable challenge to effective drug delivery. Moreover, systemic administration of nanotherapies often leads to their premature clearance by the mononuclear phagocyte system, resulting in the unsatisfying pharmacokinetics and drug concentrations within lesions [57]. Contemporarily, cell membrane-camouflaged nanotechnology has been regarded as a promising drug delivery platform for immune-related diseases, because natural cell membrane-coated nanoparticles could increase penetration and accumulation of drugs in situ, prolong circulation and half life, activate targeting ability [58]. Noteworthily, macrophage membranes-based nanoparticles present unique advantages because of their self-recognition capacity, including enhanced anti-phagocytosis ability by dendritic cells and macrophage, and improved lesion tissues targeting bias [29]. To improve the bio-utilization of 2-APB, we have constructed a nanotherapeutic delivery platform that employed macrophage membranes, thereby addressing the issues of large dosing requirements, poor targeting, and rapid drug clearance of 2-APB. In addition, both our experiments in vitro and in vivo have demonstrated their good biosafety profile of our 2-APB@DGP-MM nanotherapy system, which specifically targeting macrophages and exhibiting excellent anti-inflammation effect.

In our current study, we extracted macrophage membranes from macrophages, carefully preserving their composition and antigens. The resultant nanotherapy system possesses several unique characteristics and functionalities of their native cells, such as the ability to neutralize pathological molecules, evade immune responses, circulate for extended periods, and selectively accumulate at the affected site. We synthesized DGP, a molecule that can be specifically recognized and cleaved by MMP2, and successfully conjugated the D-terminus of 2-APB on it, resulting in the formation of 2-APB@DGP. This drug delivery system was then coated with the extracted macrophage membrane to form the final 2-APB@DGP-MM nanotherapy system. Upon injection into the ankle joints of CIA model mice, this system acted in two ways. The inflammatory joint environment facilitated degradation of the macrophage membrane, exposing 2-APB@DGP to the site of inflammation, where MMP2 cleaved DGP to release 2-APB. Simultaneously, the endogenous macrophage membranes allowed 2-APB@DGP-MM to be internalized by synovial macrophages, thereby targeting these cells and further releasing 2-APB, which has the potential to regulate macrophage polarization, and consequently alleviate RA.

## Conclusion

In summary, our development of 2-APB@DGP-MM nanotherapeutic system has demonstrated its substantial potential in alleviating inflammation by reducing

pro-inflammatory M1 macrophages percentage and promoting anti-inflammatory M2 macrophages, offering promising therapeutic opportunity for RA. The system ensures targeted release of 2-APB within inflamed joints and improves its bioavailability. We have proven that the intra-articular injection of 2-APB@DGP-MM can significantly reduce synovial inflammation and cartilage destruction in CIA mice, highlighting the substantial promise of the 2-APB@DGP-MM nanotherapeutic system for RA treatment.

## Supplementary Information

The online version contains supplementary material available at https://doi.org/10.1186/s12951-024-02822-9.

Supplementary Material 1.

Supplementary Material 2.

### Author contributions

RPZ, SX and YZC contributed equally to this work. WH, CHD, YJZ, RPZ and SX conceived the idea and designed the experiments. SX, YZC, YC, YW, JX, HL, YCX, YL, ZJP, SFL, JD, KW and FY completed the experiments. SX, YZC and KW performed the data analysis and statistical evaluation. RPZ, SX, YZC and XW wrote the manuscript and revised the manuscript. All authors reviewed the manuscript.

### Funding

This work was supported by grants from the National Natural Science Foundation of China (No. 82272450, No. 82371575), and the Outstanding Youth Project of Anhui Provincial Natural Science Foundation (2308085Y44).

### Data availability

All data in this study are available from the corresponding author upon reasonable request. No datasets were generated or analysed during the current study.

## Declarations

### Ethics approval and consent to participate

The animal experimental operation was performed at the Institute of Health and Medicine, Hefei Comprehensive National Science Center. All animal experiments had been reviewed and approved by the Laboratory Animal Ethics Committee of Anhui Medical University (Anhui, China) (Approval No. LLSC20190062).

### Competing interests

The authors declare no competing interests.

### Author details

[1]Department of Clinical Pharmacology, The Second Affiliated Hospital of Anhui Medical University, Hefei 230601, China. [2]The Key Laboratory of Major Autoimmune Diseases, School of Pharmacy, Anhui Institute of Innovative Drugs, Anhui Medical University, Hefei 230032, China. [3]The Key Laboratory of Anti-Inflammatory and Immune Medicine, Anhui Medical University, Ministry of Education, Hefei 230032, China. [4]Department of Sports Medicine, Peking University Shenzhen Hospital, Shenzhen Peking University-The Hong Kong University of Science and Technology Medical Center, Shenzhen 518036, China. [5]Clinical Research Centre, Zhujiang Hospital, Southern Medical University, Guangzhou 510200, China. [6]Division of Life Sciences and Medicine, The First Affiliated Hospital of USTC, University of Science and Technology of China, Hefei 230001, People's Republic of China. [7]Menzies Institute for Medical Research, University of Tasmania, Hobart, TAS, Australia.

Received: 26 May 2024 Accepted: 30 August 2024
Published online: 19 September 2024

### References

1. Smolen JS, Aletaha D, McInnes IB. Rheumatoid arthritis. Lancet. 2016;388:2023–38.
2. Diseases GBD, Injuries C. Global burden of 369 diseases and injuries in 204 countries and territories, 1990–2019: a systematic analysis for the Global Burden of Disease Study 2019. Lancet. 2020;396:1204–22.
3. Fan XX, Xu MZ, Leung EL, Jun C, Yuan Z, Liu L. ROS-responsive berberine polymeric micelles effectively suppressed the inflammation of rheumatoid arthritis by targeting mitochondria. Nanomicro Lett. 2020;12:76.
4. Fan Z, Li J, Liu J, Jiao H, Liu B. Anti-inflammation and joint lubrication dual effects of a novel hyaluronic acid/curcumin nanomicelle improve the efficacy of rheumatoid arthritis therapy. ACS Appl Mater Interfaces. 2018;10:23595–604.
5. Asquith DL, Ballantine LE, Nijjar JS, Makdasy MK, Patel S, Wright PB, Reilly JH, Kerr S, Kurowska-Stolarska M, Gracie JA, McInnes IB. The liver X receptor pathway is highly upregulated in rheumatoid arthritis synovial macrophages and potentiates TLR-driven cytokine release. Ann Rheum Dis. 2013;72:2024–31.
6. Yang Y, Guo L, Wang Z, Liu P, Liu X, Ding J, Zhou W. Targeted silver nanoparticles for rheumatoid arthritis therapy via macrophage apoptosis and Re-polarization. Biomaterials. 2021;264: 120390.
7. Chambers M, Rees A, Cronin JG, Nair M, Jones N, Thornton CA. Macrophage plasticity in reproduction and environmental influences on their function. Front Immunol. 2020;11: 607328.
8. Wang Q, Jiang H, Li Y, Chen W, Li H, Peng K, Zhang Z, Sun X. Targeting NF-kB signaling with polymeric hybrid micelles that co-deliver siRNA and dexamethasone for arthritis therapy. Biomaterials. 2017;122:10–22.
9. Lawrence T, Natoli G. Transcriptional regulation of macrophage polarization: enabling diversity with identity. Nat Rev Immunol. 2011;11:750–61.
10. Jain S, Tran TH, Amiji M. Macrophage repolarization with targeted alginate nanoparticles containing IL-10 plasmid DNA for the treatment of experimental arthritis. Biomaterials. 2015;61:162–77.
11. Rosalez MN, Estevez-Fregoso E, Alatorre A, Abad-Garcia A. M AS-U: 2-aminoethyldiphenyl borinate: a multitarget compound with potential as a drug precursor. Curr Mol Pharmacol. 2020;13:57–75.
12. Nielsen FH. Is boron nutritionally relevant? Nutr Rev. 2008;66:183–91.
13. Gorustovich AA, Steimetz T, Nielsen FH, Guglielmotti MB. Histomorphometric study of alveolar bone healing in rats fed a boron-deficient diet. Anat Rec. 2008;291:441–7.
14. Nielsen FH, Stoecker BJ. Boron and fish oil have different beneficial effects on strength and trabecular microarchitecture of bone. J Trace Elem Med Biol. 2009;23:195–203.
15. Zofkova I, Nemcikova P, Matucha P. Trace elements and bone health. Clin Chem Lab Med. 2013;51:1555–61.
16. Miljkovic D, Scorei RI, Cimpoiasu VM, Scorei ID. Calcium fructoborate: plant-based dietary boron for human nutrition. J Diet Suppl. 2009;6:211–26.
17. Scorei RI, Ciofrangeanu C, Ion R, Cimpean A, Galateanu B, Mitran V, Iordachescu D. In vitro effects of calcium fructoborate upon production of inflammatory mediators by LPS-stimulated RAW 264.7 macrophages. Biol Trace Elem Res. 2010;135:334–44.
18. Bilmen JG, Wootton LL, Godfrey RE, Smart OS, Michelangeli F. Inhibition of SERCA Ca2+ pumps by 2-aminoethoxydiphenyl borate (2-APB). 2-APB reduces both Ca2+ binding and phosphoryl transfer from ATP, by interfering with the pathway leading to the Ca2+-binding sites. Eur J Biochem. 2002;269:3678–87.
19. McCain J. The MAPK (ERK) pathway: investigational combinations for the treatment of BRAF-mutated metastatic melanoma. Pharm Ther. 2013;38:96–108.
20. Eapen A, Ramachandran A, Pratap J, George A. Activation of the ERK1/2 mitogen-activated protein kinase cascade by dentin matrix protein 1 promotes osteoblast differentiation. Cells Tissues Organs. 2011;194:255–60.

21. Tanaka T, Narazaki M, Kishimoto T. IL-6 in inflammation, immunity, and disease. Cold Spring Harb Perspect Biol. 2014;6: a016295.
22. Uhl B, Vadlau Y, Zuchtriegel G, Nekolla K, Sharaf K, Gaertner F, Massberg S, Krombach F, Reichel CA. Aged neutrophils contribute to the first line of defense in the acute inflammatory response. Blood. 2016;128:2327–37.
23. Conejeros I, Jara E, Carretta MD, Alarcon P, Hidalgo MA, Burgos RA. 2-Aminoethoxydiphenyl borate (2-APB) reduces respiratory burst, MMP-9 release and CD11b expression, and increases l-selectin shedding in bovine neutrophils. Res Vet Sci. 2012;92:103–10.
24. Zhou R, Chen Y, Li S, Wei X, Hu W, Tang S, Ding J, Fu W, Zhang H, Chen F, et al. TRPM7 channel inhibition attenuates rheumatoid arthritis articular chondrocyte ferroptosis by suppression of the PKCalpha-NOX4 axis. Redox Biol. 2022;55: 102411.
25. Zhou RP, Chen Y, Wei X, Yu B, Xiong ZG, Lu C, Hu W. Novel insights into ferroptosis: implications for age-related diseases. Theranostics. 2020;10:11976–97.
26. Zhou K, Yang C, Shi K, Liu Y, Hu D, He X, Yang Y, Chu B, Peng J, Zhou Z, Qian Z. Activated macrophage membrane-coated nanoparticles relieve osteoarthritis-induced synovitis and joint damage. Biomaterials. 2023;295: 122036.
27. Yan H, Shao D, Lao YH, Li M, Hu H, Leong KW. Engineering cell membrane-based nanotherapeutics to target inflammation. Adv Sci. 2019;6:1900605.
28. Tan S, Wu T, Zhang D, Zhang Z. Cell or cell membrane-based drug delivery systems. Theranostics. 2015;5:863–81.
29. Huang X, Wang L, Guo H, Zhang W. Macrophage membrane-coated nanovesicles for dual-targeted drug delivery to inhibit tumor and induce macrophage polarization. Bioact Mater. 2023;23:69–79.
30. Zhou R, Fu W, Vasylyev D, Waxman SG, Liu CJ. Ion channels in osteoarthritis: emerging roles and potential targets. Nat Rev Rheumatol. 2024;20:545–64.
31. Zhang Q, Dehaini D, Zhang Y, Zhou J, Chen X, Zhang L, Fang RH, Gao W, Zhang L. Neutrophil membrane-coated nanoparticles inhibit synovial inflammation and alleviate joint damage in inflammatory arthritis. Nat Nanotechnol. 2018;13:1182–90.
32. Ying K, Zhu Y, Wan J, Zhan C, Wang Y, Xie B, Xu P, Pan H, Wang H. Macrophage membrane-biomimetic adhesive polycaprolactone nanocamptothecin for improving cancer-targeting efficiency and impairing metastasis. Bioact Mater. 2023;20:449–62.
33. Rui K, Zhang Z, Tian J, Lin X, Wang X, Ma J, Tang X, Xu H, Lu L, Wang S. Olfactory ecto-mesenchymal stem cells possess immunoregulatory function and suppress autoimmune arthritis. Cell Mol Immunol. 2016;13:401–8.
34. Zhai Z, Yang F, Xu W, Han J, Luo G, Li Y, Zhuang J, Jie H, Li X, Shi X, et al. Attenuation of rheumatoid arthritis through the inhibition of tumor necrosis factor-induced caspase 3/gasdermin E-mediated pyroptosis. Arthritis Rheumatol. 2022;74:427–40.
35. Tu J, Chen W, Fang Y, Han D, Chen Y, Jiang H, Tan X, Xu Z, Wu X, Wang H, et al. PU.1 promotes development of rheumatoid arthritis via repressing FLT3 in macrophages and fibroblast-like synoviocytes. Ann Rheum Dis. 2023;82:198–211.
36. Cutolo M, Campitiello R, Gotelli E, Soldano S. The role of M1/M2 macrophage polarization in rheumatoid arthritis synovitis. Front Immunol. 2022;13: 867260.
37. Cui S, Wu Q, Wang J, Li M, Qian J, Li S. Quercetin inhibits LPS-induced macrophage migration by suppressing the iNOS/FAK/paxillin pathway and modulating the cytoskeleton. Cell Adhes Migr. 2019;13:1–12.
38. Lardner A. The effects of extracellular pH on immune function. J Leukoc Biol. 2001;69:522–30.
39. Wu H, Yin Y, Hu X, Peng C, Liu Y, Li Q, Huang W, Huang Q. Effects of environmental pH on macrophage polarization and osteoimmunomodulation. ACS Biomater Sci Eng. 2019;5:5548–57.
40. McWhorter FY, Wang T, Nguyen P, Chung T, Liu WF. Modulation of macrophage phenotype by cell shape. Proc Natl Acad Sci U S A. 2013;110:17253–8.
41. Waldo SW, Li Y, Buono C, Zhao B, Billings EM, Chang J, Kruth HS. Heterogeneity of human macrophages in culture and in atherosclerotic plaques. Am J Pathol. 2008;172:1112–26.
42. Dong L, Zhao Y, Sun C, Ou Yang Z, Chen F, Hu W, Zhang H, Wang Y, Zhu R, Cheng Y, et al. ASIC1a-CMPK2-mediated M1 macrophage polarization exacerbates chondrocyte senescence in osteoarthritis through IL-18. Int Immunopharmacol. 2023;124: 110878.
43. Xuan M, Shao J, Dai L, He Q, Li J. Macrophage cell membrane camouflaged mesoporous silica nanocapsules for in vivo cancer therapy. Adv Healthc Mater. 2015;4:1645–52.
44. Xuan M, Shao J, Dai L, Li J, He Q. Macrophage cell membrane camouflaged Au nanoshells for in vivo prolonged circulation life and enhanced cancer photothermal therapy. ACS Appl Mater Interfaces. 2016;8:9610–8.
45. Taylor PR, Martinez-Pomares L, Stacey M, Lin HH, Brown GD, Gordon S. Macrophage receptors and immune recognition. Annu Rev Immunol. 2005;23:901–44.
46. Diab A, Abdalla H, Li HL, Shi FD, Zhu J, Hojberg B, Lindquist L, Wretlind B, Bakhiet M, Link H. Neutralization of macrophage inflammatory protein 2 (MIP-2) and MIP-1alpha attenuates neutrophil recruitment in the central nervous system during experimental bacterial meningitis. Infect Immun. 1999;67:2590–601.
47. Shi Y, Xie F, Rao P, Qian H, Chen R, Chen H, Li D, Mu D, Zhang L, Lv P, et al. TRAIL-expressing cell membrane nanovesicles as an anti-inflammatory platform for rheumatoid arthritis therapy. J Control Release. 2020;320:304–13.
48. Shi M, Shen K, Yang B, Zhang P, Lv K, Qi H, Wang Y, Li M, Yuan Q, Zhang Y. An electroporation strategy to synthesize the membrane-coated nanoparticles for enhanced anti-inflammation therapy in bone infection. Theranostics. 2021;11:2349–63.
49. Ostrowska M, Maslinski W, Prochorec-Sobieszek M, Nieciecki M, Sudol-Szopinska I. Cartilage and bone damage in rheumatoid arthritis. Reumatologia. 2018;56:111–20.
50. Wang M, Liu C, Thormann E, Dėdinaitė A. Hyaluronan and phospholipid association in biolubrication. Biomacromol. 2013;14:4198–206.
51. Ye L, Wen Z, Li Y, Chen B, Yu T, Liu L, Zhang J, Ma Y, Xiao S, Ding L, et al. Interleukin-10 attenuation of collagen-induced arthritis is associated with suppression of interleukin-17 and retinoid-related orphan receptor gammat production in macrophages and repression of classically activated macrophages. Arthritis Res Ther. 2014;16:R96.
52. Edilova MI, Akram A, Abdul-Sater AA. Innate immunity drives pathogenesis of rheumatoid arthritis. Biomed J. 2021;44:172–82.
53. Zhou RP, Liang HY, Hu WR, Ding J, Li SF, Chen Y, Zhao YJ, Lu C, Chen FH, Hu W. Modulators of ASIC1a and its potential as a therapeutic target for age-related diseases. Ageing Res Rev. 2023;83: 101785.
54. Yang X, Zhao Y, Wei Q, Zhu X, Wang L, Zhang W, Liu X, Kuai J, Wang F, Wei W. GRK2 inhibits Flt-1(+) macrophage infiltration and its proangiogenic properties in rheumatoid arthritis. Acta Pharm Sin B. 2024;14:241–55.
55. Lin Y, Chen Y, Hu W, Liu X, Hao W, Xing J, Ding J, Xu Y, Yao F, Zhao Y, et al. TRPM7 facilitates fibroblast-like synoviocyte proliferation, metastasis and inflammation through increasing IL-6 stability via the PKCalpha-HuR axis in rheumatoid arthritis. Int Immunopharmacol. 2024;132: 111933.
56. Culemann S, Gruneboom A, Nicolas-Avila JA, Weidner D, Lammle KF, Rothe T, Quintana JA, Kirchner P, Krljanac B, Eberhardt M, et al. Locally renewing resident synovial macrophages provide a protective barrier for the joint. Nature. 2019;572:670–5.
57. Buckley CD, Ospelt C, Gay S, Midwood KS. Location, location, location: how the tissue microenvironment affects inflammation in RA. Nat Rev Rheumatol. 2021;17:195–212.
58. Huang X, Zhang W. Macrophage membrane-camouflaged biomimetic nanovesicles for targeted treatment of arthritis. Ageing Res Rev. 2024;95: 102241.


## Publisher's Note